Astron. Astrophys. 363, 825–836 (2000)

ASTRONOMY AND ASTROPHYSICS

On the detection of neutrino oscillations with Planck surveyor

L. Popa[1,2], **C. Burigana**[2], **F. Finelli**[2,3⋆], **and N. Mandolesi**[2]

[1] Institute of Space Sciences, 76900 Bucharest-Magurele, Romania
[2] Istituto TeSRE, Consiglio Nazionale delle Ricerche, Via Gobetti 101, 40129 Bologna, Italy
[3] University of Bologna and INFN, Via Irnerio 46, 40126 Bologna, Italy

Received 6 March 2000 / Accepted 28 September 2000

Abstract. The imprint of neutrino oscillations on the Cosmic Microwave Background (CMB) anisotropy and polarization power spectra is evaluated in a ΛCHDM model with two active neutrino flavors, consistent with the structure formation models and the atmospheric neutrino oscillations data.

By using the Fisher information matrix method we find that the neutrino oscillations could be detected by PLANCK surveyor if the present value of the lepton asymmetry $L_\nu \geq 4.5 \times 10^{-3}$, the difference of the neutrino squared masses $\Delta m^2 \geq 9.7 \times 10^{-3}\mathrm{eV}^2$ and the vacuum mixing angle $\sin^2 2\theta_0 \geq 0.13$, showing the existence of a significant overlap between the region of the oscillation parameter space that can be measured by PLANCK surveyor and that implied by the atmospheric neutrino oscillations data.

Key words: cosmology: cosmic microwave background – cosmology: dark matter – cosmology: large-scale structure of Universe – elementary particles

1. Introduction

The atmospheric neutrino results from Super-Kamiokande (Fukuda et al. 1998) and MACRO (Ambrosio et al. 1998) experiments indicate that neutrinos oscillate. Those data are consistent with $\nu_\mu \leftrightarrow \nu_\tau$ oscillations, but do not exclude ν_μ oscillations to a sterile neutrino ν_s (see e.g. Foot et al. 1996; Foot & Volkas 1997, 1999). The small value of the difference of the squared masses ($5 \times 10^{-4}\mathrm{eV}^2 \leq \Delta m^2 \leq 6 \times 10^{-3}\mathrm{eV}^2$) and the strong mixing angle ($\sin^2 2\theta \geq 0.82$) suggest that these neutrinos are nearly equal in mass as predicted by many models of particle physics beyond the standard model (see e.g. Primack & Gross 1998 and the references therein). Also, the LSND experiment (Athanassopoulos et al. 1998) support $\nu_\mu \leftrightarrow \nu_e$ oscillations with $\Delta m^2 \leq 0.2\mathrm{eV}^2$ and other different types of solar neutrino experiments (Bahcall et al. 1998) suggest that ν_e could oscillate to a sterile neutrino $\nu_e \leftrightarrow \nu_s$ with $\Delta m^2 \simeq 10^{-5}\mathrm{eV}^2$.

Send offprint requests to: lpopa@venus.nipne.ro or popa@tesre.bo.cnr.it

⋆ *Present address:* Purdue University, Physics Department, West Lafayette, IN 47907-1396, USA

The direct implication of neutrino oscillations is the existence of non-zero neutrino masses in the eV range, and consequently a not negligible hot dark matter contribution to the total mass density of the universe (i.e. a density parameter $\Omega_\nu \neq 0$).

In view of the uncertainty in the direct neutrino experiments, a possible significant contribution can be obtained from the study of the cosmological implications of neutrino oscillations. In particular, the Cosmic Microwave Background (CMB) anisotropy pattern reflects the conditions in the universe at the time of the last scattering between photons and electrons, occurring at a redshift $z \approx 1000$ for standard recombination models. This means that all the physical processes occurring before this epoch could have left imprints on the CMB angular power spectra.

The standard Cold Dark Matter (CDM) model normalized to COBE/DMR data (Smoot et al. 1992; Wright et al. 1994; Górski et al. 1994; Bennett et al. 1996a) predicts both the amplitude and the shape of the CMB power spectrum at small scales inconsistent with the observations of the Large Scale Structure (LLS) of the universe as derived by galaxy surveys (e.g. Scott & White 1994; White et al. 1995; Primack et al. 1995). Recent works (Primack 1998; Gawiser & Silk 1998) show that the Cold + Hot Dark Matter (CHDM) model is the single model with $\Omega_m = 1$ whose predictions agree with both LSS observations and current CMB anisotropies data. The Cν^2DM model (Primack et al. 1995) with two 2.4eV neutrinos contributing with 20% to the total density of the universe and with another 80% contribution from cold dark matter and a small baryon fraction, agrees remarkably with all available observations only if the Hubble parameter is $H_0 = 50$ km s^{-1}Mpc^{-1} ($h_0 = H_0/100$ km s^{-1}Mpc$^{-1} = 0.5$).

However, increasing evidence for larger value of the Hubble parameter, $h_0 \simeq 0.6 - 0.8$, (see e.g. Fukugita et al. 1999 and the references therein) are inconsistent with standard CHDM models. Such high values of the Hubble parameter make an $\Omega_m = 1$ universe suspiciously young unless the cosmological constant is non-zero. A way to improve the agreement of the standard CHDM models with eV neutrino mass with high values of Hubble parameter is to consider the relic neutrino degeneracy (the degeneracy parameter is defined as: $\xi_\nu = \mu_\nu/T_\nu$, where μ_ν is the neutrino chemical potential and T_ν is the neutrino temperature), that enhances the contribution of neutrinos to the total

energy density of the universe (Larsen & Madsen 1995). The cosmological implications of the neutrino degeneracy has been often considered in the literature: it can change the neutrino decoupling temperature (Freese et al. 1983; Kang & Steigman 1992), the abundances of light elements at the big bang nucleosynthesis (BBN) (Steigman et al. 1977; Kang & Steigman 1992), the CMB anisotropies and the matter power spectrum (Kinney & Riotto 1999). For the CHDM models with degenerated neutrinos, the increase of the neutrino chemical potential increases the effective number of neutrino species in the relativistic era (Larsen & Madsen 1995; Hannestad 2000), and can bring the power spectral shape parameter in the range required by observations [for CDM models with low baryonic content the power spectral shape parameter (which basically measures the horizon scale at matter-radiation equality) is defined as (Dodelson et al. 1994): $\Gamma \approx \Omega_m h_0 (g_*/3.36)^{-1/2}$, where g_* counts the relativistic degrees of freedom and $g_* = 3.36$ corresponds to the standard model with photons and three massless neutrino species; observations require $0.22 < \Gamma < 0.29$]. The free-streaming properties of degenerated neutrinos also differ: when the neutrino chemical potential is increased, the neutrino number density is higher, although the neutrino energy density and the mean momentum change a little. The effect is the increase of the radiation energy density and the delay of the matter-radiation equality. It is shown (Larsen & Madsen 1995) that an $\Omega_m = 1$ CHDM model with one 2.4eV neutrino and $h_0 = 0.7$ is in good agreement with the observed LSS power spectrum of density fluctuations if the neutrino degeneracy parameter is $\xi_\nu \approx 2.8$. Constraints on neutrino degeneracy coming from BBN (Kang & Steigman 1992) indicate $-0.06 \leq \xi_{\nu_e} \leq 1.1$ and $|\xi_{\nu_{\mu,\tau}}| \leq 6.9$. Recent works (Pal & Kar 1999; Lesgourgues & Pastor 1999; Kinney & Riotto 1999; Lesgourgues et al. 1999) derive bounds on neutrino degeneracy parameter in agreement with BBN predictions, by combining the current observations of the CMB anisotropies and LSS data. The likelihood analysis of the CMB anisotropy data obtained by the Boomerang experiment indicates bounds on massless neutrino degeneracy parameter (Hannestad 2000) of $|\xi_{\nu_{e,\mu,\tau}}| \leq 3.7$ if only one massless neutrino species is degenerated and $|\xi_\nu| \leq 2.4$ if the asymmetry is equally shared among three massless species.

On the other hand, evidences have been accumulated that we live in a low matter density universe (see e.g. Fukugita et al. 1999 and the references therein). Indications like Hubble diagram of Type 1a supernovae (Riess et al. 1998; Perlmutter et al. 1997) and the acoustic peak distribution in the CMB anisotropy power spectra (Hancock et al. 1998; Efstathiou et al. 1999) point to a universe dominated by vacuum energy (cosmological constant Λ) that keeps the universe close to flat. The combined analysis of the latest CMB anisotropy data and Type 1a supernovae data (Efstathiou et al. 1999) indicates $\Omega_m = 0.25^{+0.18}_{-0.12}$ and $\Omega_\Lambda = 0.63^{+0.17}_{-0.23}$ (95% confidence errors) for matter and vacuum energy densities respectively. These values are close to those favoured by other arguments (see e.g. Efstathiou et al. 1999 and the references therein) like the ages of globular clusters, observations of large scale structure, baryon abundance in clusters.

Adding a Hot Dark Matter component to the ΛCDM model (ΛCHDM) leads to a worse fit to LSS and CMB data, resulting in a limit on the total neutrino mass (Gawiser 2000) of $m_\nu \leq 2$eV for a primordial scale invariant power spectrum and $m_\nu \leq 4$eV for a primordial scale free power spectrum. A stronger upper limit is obtained (Fukugita et al. 1999) from the matching condition of the LSS power spectrum normalization σ_8 (defined as the *rms* amplitude of the galaxy power spectrum in a sphere of radius $8h_0^{-1}$Mpc) at the COBE scale and at the cluster scale. For the case of a ΛCHDM model having $\Omega_m = 0.3$, $\Omega_\Lambda = 0.7$, and a primordial scale invariant power spectrum, it is found an upper limit of the total non-degenerated neutrino mass of $m_\nu < 0.6$ if the Hubble constant $H_0 < 80$ Km s^{-1} Mpc^{-1}.

In this paper we study the signature of relic degenerated neutrino oscillations on the CMB anisotropy and polarization power spectra and address its detectability with the future CMB anisotropy space missions, MAP (Microwave Anisotropy Probe) (see Bennett et al. 1996b) and PLANCK (Mandolesi et al. 1998a; Puget et al. 1998). We consider the impact of neutrino oscillations in the epoch after nucleosynthesis. Neutrino oscillations are mediated by weak interactions: this fact implies that the order of magnitude of the interaction rate is less than the Hubble expansion rate after nucleosynthesis. In order to get an appreciable effect we consider a large neutrino asymmetry as left by processes occurred before and during nucleosynthesis. An example of such large asymmetries is given by considering a relic neutrino degeneracy (Larsen & Madsen 1995), which has been recently subject of renewed interest (Kinney & Riotto 1999; Lesgourges & Pastor 1999; Pal & Kar 1999). We analyze the oscillations of relic degenerated neutrinos under the simple assumption of oscillations occurring between two active neutrino flavors

$$\nu_\mu \leftrightarrow \nu_\tau \qquad \bar{\nu}_\mu \leftrightarrow \bar{\nu}_\tau$$

which have the following mass hierarchy:

$$m_{\nu_\tau} = m_{\bar{\nu}_\tau} > m_{\nu_\mu} = m_{\bar{\nu}_\mu}$$

We assume the third neutrino ν_e as massless and non-degenerate. We consider a total neutrino mass contribution of $m_\nu = m_{\nu_\mu} + m_{\nu_\tau} = 0.6$ eV and a total neutrino degeneracy parameter $\xi_\nu = |\xi_{\nu_\mu} + \xi_{\nu_\tau}| \leq 5$ accordingly to the present observational data summarized above. We assume a scale invariant primordial power spectrum, the presence of the scalar modes with spectral index $n_s = 1$ and ignore the contribution of the tensorial modes and the reionisation effects. This model is consistent with the large scale structure and CMB anisotropy data, allowing in the same time a pattern of neutrino masses consistent with the results from atmospheric neutrino oscillations experiments.

In Sect. 2 we draw the basic formalism of the neutrino oscillation model necessary for understanding its impact on CMB angular power spectra. The features induced by the degenerated neutrino oscillations on the CMB anisotropy and polarization power spectra are presented in Sect. 3. In Sect. 4 we discuss the MAP and PLANCK capability of detecting neutrino oscillations. Finally, we summarize our main conclusions in Sect. 5.

Throughout the paper we employ the system of units in which $\hbar = c = k_B = 1$.

2. Oscillations of degenerated neutrinos

The neutrino oscillations take place due to the fact that neutrino mass eigenstate components propagate differently because they have different energies, momenta and masses. In the standard assumption of the mixing of massive neutrinos, the neutrino flavor eigenstates are described by a superposition of the mass eigenstate components (Particle Data Group 1998). For oscillations occurring in vacuum between two neutrino flavors ν_μ and ν_τ the mixing can be written as:

$$\begin{aligned} |\nu_\mu\rangle &= \cos\theta_0|\nu_2\rangle + \sin\theta_0|\nu_3\rangle \\ |\nu_\tau\rangle &= -\sin\theta_0|\nu_2\rangle + \cos\theta_0|\nu_3\rangle, \end{aligned} \quad (1)$$

where ν_2 and ν_3 are the mass eigenstate components and θ_0 is the vacuum mixing angle. The mixing of antineutrinos can be obtained from Eq. (1) by performing the transformations $\nu_\mu \leftrightarrow \bar{\nu}_\mu$ and $\nu_\tau \leftrightarrow \bar{\nu}_\tau$. It is usual to consider that each neutrino/antineutrino of a definite flavor is dominantly one mass eigenstate (Particle Data Group 1998). In this circumstance we refer to the dominant mass eigenstate component of $\nu_\mu/\bar{\nu}_\mu$ as ν_2, that of $\nu_\tau/\bar{\nu}_\tau$ as ν_3 and to their difference of the squared masses as $\Delta m^2 = m_3^2 - m_2^2$.

The mixing of the mass eigenstate components are modified in the presence of the asymmetric background. The background mixing angle and the vacuum mixing angle are related through (see e.g. Foot et al. 1996):

$$\sin^2 2\theta_m = \frac{\sin^2 2\theta_0}{1 - 2z\cos 2\theta_0 + z^2}. \quad (2)$$

Here $z = 2\langle p\rangle \langle V_{\nu_i}\rangle / \Delta m^2$ $(i = \mu, \tau)$, $\langle p\rangle$ is the averaged neutrino momentum and $\langle V_{\nu_i}\rangle$ is the neutrino effective potential due to the interaction with the asymmetric background (Enqvist et al. 1992; Foot et al. 1996):

$$\langle V_{\nu_i}\rangle = \sqrt{2} G_F n_\gamma \left(L^i - A_{\nu_i} \frac{pT_\nu}{4M_Z^2} [n_{\nu_i} + n_{\bar{\nu}_i}] \right), \quad (3)$$

where A_{ν_i} is a numerical factor ($A_{\mu,\tau} = 12.61$), T_ν is the neutrino temperature, G_F is the Fermi constant ($G_F = 1.17 \times 10^{-11} MeV^{-2}$) M_Z is the mass of Z boson, ($M_Z = 91.187$GeV), n_γ is the photon number density ($n_\gamma \simeq T^3/4.1$), n_{ν_i} and $n_{\bar{\nu}_i}$ are the neutrino and antineutrino number densities.

The functions L^i are defined as (Foot et al. 1996; Foot & Volkas 1997):

$$L^i = L_{\nu_i} + L_{\nu_\mu} + L_{\nu_\tau} + L_{\nu_e} + L_e + \eta \qquad (i = \mu, \tau) \quad (4)$$

Here η is approximately equal to the baryon to photon ratio, and $L^{'}$s are the lepton asymmetries defined as:

$$L_\alpha = \frac{n_\alpha - n_{\bar{\alpha}}}{n_\gamma}, \quad (5)$$

where $n^{'}$s are the number densities.

For the purpose of this work we consider large neutrino asymmetries ($L_{\nu_i} \geq 10^{-9}$). Also, we consider that ν_e is non-degenerated and consequently $L_{\nu_e} = 0$. In this case the functions L^i may be written as:

$$L^i \simeq L_{\nu_i} + L_{\nu_\mu} + L_{\nu_\tau}. \quad (6)$$

The effective potentials of antineutrinos can be obtained by replacing L^i with $-L^i$ in Eq. (3).

The neutrino flavor eigenstates oscillate via weak interaction processes. The average oscillation probability $\langle \mathcal{P}\rangle_{\nu_i}$ of a flavor eigenstate $|\nu_i\rangle$ $(i = \mu, \tau)$ is defined as (see e.g.: Raffelt 1996; Foot et al.1996; Enqvist et al. 1992):

$$\langle \mathcal{P}\rangle_{\nu_i} = \sin^2 2\theta_m \left\langle \sin^2 \frac{L_{int}}{L_{osc}} \right\rangle \Gamma_{coll}(\nu_i \to \nu_j) \qquad (i = \mu, \tau \;\; j = \mu, \tau \;\; i \neq j), \quad (7)$$

where $\Gamma_{coll}(\nu_i \to \nu_j)$ is the neutrino averaged elastic collision rate, L_{int} is the mean distance between interactions (Foot et al. 1996), and the neutrino oscillation length L_{osc} is given by (see e.g. Raffelt 1996):

$$L_{osc} = \frac{4\pi E_{\nu_i}}{\Delta m^2} \simeq 248\mathrm{cm} \frac{E_{\nu_i}}{\mathrm{MeV}} \frac{\mathrm{eV}^2}{\Delta m^2}, \quad (8)$$

where E_{ν_i} is the neutrino energy. We will consider the $L_{int} \gg L_{osc}$ and then $\left\langle \sin^2(L_{int}/L_{osc})\right\rangle \to 1/2$ (Foot et al. 1996). The averaged collision rate is given by (Enqvist et al. 1992):

$$\Gamma(\nu_i \to \nu_j) = 0.77 G_F^2 T_\nu^5 \frac{n_{\nu_i}}{n_0}, \quad (9)$$

where n_0 is the number density of massless non-degenerated neutrino species.

Eq. (7) together with Eqs. (2), (8), (9) gives the averaged oscillation probability $\langle \mathcal{P}\rangle_{\nu_i}$ used in the next section to evolve in time the neutrino distribution functions. The oscillation probabilities of antineutrinos can be obtained by performing the transformations $\nu_i \leftrightarrow \bar{\nu}_i$ and $\nu_j \leftrightarrow \bar{\nu}_j$ in Eqs. (7)–(9).

3. CMB angular power spectra in the presence of neutrino oscillations

The phase space distribution functions of neutrinos and antineutrinos f_{ν_i} $(i = \nu_\mu, \bar{\nu}_\mu, \nu_\tau, \bar{\nu}_\tau)$ are evolved independently, taking into account the redistribution of momenta due to oscillations and elastic collisions.

We describe the time evolution of the phase space distribution functions in the expanding universe by the set of equations:

$$\begin{aligned} \frac{\partial f_{\nu_i}(q)}{\partial t} &= -\langle \mathcal{P}\rangle_{\nu_i} f_{\nu_i}(q) + \langle \mathcal{P}\rangle_{\nu_j} f_{\nu_j}(q), \\ &\qquad (i = \mu, \tau; \;\; j = \mu, \tau; \;\; i \neq j) \\ \frac{\partial f_{\bar{\nu}_i}(q)}{\partial t} &= -\langle \mathcal{P}\rangle_{\bar{\nu}_i} f_{\bar{\nu}_i}(q) + \langle \mathcal{P}\rangle_{\bar{\nu}_j} f_{\bar{\nu}_j}(q), \end{aligned} \quad (10)$$

where $q = ap$ is the comoving momentum (Ma & Bertschinger 1995), p is the magnitude of the momentum 3-vector, a is the

scale factor ($a = 1$ today), $dt = da/(aH)$ and H is the expansion rate:

$$H = \sqrt{\frac{8\pi G\rho_{tot}(a)}{3}}, \tag{11}$$

where: G is the gravitational constant and $\rho_{tot}(a)$ is the total energy density.

The Eqs. (10) assume that no other physical processes take place apart from oscillations and elastic collisions, leading to the conservation of the total neutrino/antineutrino number densities $(n_\nu/n_{\bar\nu})$ and degeneracy parameters $(\xi_\nu/\xi_{\bar\nu})$:

$$\begin{aligned} n_\nu = n_{\nu_i} + n_{\nu_j}, \quad n_{\bar\nu} &= n_{\bar\nu_i} + n_{\bar\nu_j}, \quad (i=\mu, j=\tau) \\ \xi_\nu = \xi_{\nu_i} + \xi_{\nu_j}, \quad \xi_{\bar\nu} &= \xi_{\bar\nu_i} + \xi_{\bar\nu_j}, \end{aligned} \tag{12}$$

where $\xi_\alpha = \mu_{\nu_\alpha}/T_\nu$ is the degeneracy parameter of the flavor α ($\alpha = \mu, \tau$) with the chemical potential μ_α, T_ν is the neutrino/antineutrino temperature and $|\xi_{\bar\nu_\alpha}| = |\xi_{\nu_\alpha}|$.

We have modified the CMBFAST code (Seljak & Zaldarriaga 1996) to take into account the evolution of the phase space distribution functions of neutrinos and antineutrinos at each value of the scale factor, by solving the set of Eqs. (10). We start at the scale factor $a \simeq 10^{-9}$, when neutrinos and antineutrinos with the mass in eV range behave like relativistic particles with Fermi-Dirac phase space distributions:

$$\begin{aligned} f_{\nu_i}(q) &= \frac{1}{e^{E_{\nu_i}/T_\nu - \xi_{\nu_i}} + 1}, \quad (i = \mu, \tau) \\ f_{\bar\nu_i}(q) &= \frac{1}{e^{E_{\nu_i}/T_\nu + \xi_{\nu_i}} + 1}, \end{aligned} \tag{13}$$

where ξ_i is the degeneracy parameter, $E_{\nu_i} = \sqrt{q^2 + a^2 m_{\nu_i}^2}$ the neutrino/antineutrino energy, m_{ν_i} the dominant mass component of the flavor i, and q the comoving momentum. The system of neutrinos and antineutrinos drops out from thermal equilibrium with $e^\pm$, photons, the small fraction of baryons and other massive species (e.g. $\mu^+\mu^-$ pairs) when the ratio of the averaged weak interaction rate to the expansion rate falls below unity. The decoupling temperature of degenerated neutrinos increases exponentially with the degeneracy parameter. For ν_μ and ν_τ the decoupling temperature is given by (Freese et al. 1983; Kang & Steigmann 1992) $T_D \simeq 10$ MeV $\xi^{-2/3} e^{(\xi/3)}$.

The present values of neutrino/antineutrino temperature T_{ν_0} and photons temperature $T_0 = 2.725 \pm 0.002$K (Mather et al. 1999) are related through $T_{\nu_0}/T_0 \simeq (3.9/g_{*D})^{1/3}$ where g_{*D} is the number of degrees of freedom in equilibrium at neutrino/antineutrino decoupling. For a degeneracy parameter $\xi_\nu \leq 15$, $T_D \simeq$ few MeV and the total number of relativistic degrees of freedom is $g_* \simeq 43/4$ (Freese et al. 1983). After the neutrino decoupling, the e^+e^- pairs annihilate, heating the photons but not the neutrinos. From the entropy conservation one obtains that $T_{\nu_0} \simeq (4/11)^{1/3} T_0$ and the total degeneracy parameter $\xi_\nu = \xi_{\nu_\mu} + \xi_{\nu_\tau}$ is considered constant.

We compute the mean energy density and pressure of each neutrino flavor as:

$$\rho_{\nu_i} + \rho_{\bar\nu_i} = \frac{T_\nu^4}{2\pi^2} \int_0^\infty dq\, q^2 E_{\nu_i} (f_{\nu_i}(q) + f_{\bar\nu_i}(q)),$$

$$P_{\nu_i} + P_{\bar\nu_i} = \frac{T_\nu^4}{6\pi^2} \int_0^\infty dq\, \frac{q^2}{E_{\nu_i}} (f_{\nu_i}(q) + f_{\bar\nu_i}(q)), \quad (i = \mu, \tau) \tag{14}$$

the neutrino and antineutrino number densities:

$$n_{\nu_i} = \frac{T_\nu^4}{2\pi^2} \int_0^\infty dq\, q^2 f_{\nu_i}(q), \quad n_{\bar\nu_i} = \frac{T_\nu^4}{2\pi^2} \int_0^\infty dq\, q^2 f_{\bar\nu_i}(q), \quad (i = \mu, \tau) \tag{15}$$

and the present lepton asymmetry in the form of neutrinos (Kang & Steigmann 1992):

$$L_\nu = \sum_{i=\mu,\tau} \frac{1}{12\zeta(3)} \frac{T_{\nu_0}}{T_0} [\xi_{\nu_i} + \pi^2 \xi_{\nu_i}]. \tag{16}$$

We also compute at the beginning of the code the present value of neutrino parameter density:

$$\Omega_\nu = \sum_{i=\mu,\tau} \frac{(\rho_{\nu_i} + \rho_{\bar\nu_i})_{a=1}}{\rho_c}, \tag{17}$$

where $\rho_c = 1.054 \times 10^4 h_0^2$ eV cm^{-3} is the critical density, and define the cold dark matter density parameter $\Omega_c = 1 - \Omega_b - \Omega_\nu - \Omega_\Lambda$.

Following the same procedure used by the CMBFAST code, we compute in synchronous gauge the perturbations of the energy density, pressure, energy flux and shear stress (Eqs. (52)–(56) from Ma & Bertschinger 1995) for neutrinos and antineutrinos of each flavor.

We performed the computations of the CMB anisotropy and polarization power spectra starting with $N_{q_{max}} = 15$ equispaced sampling points of the phase space distribution functions and truncating the Boltzmann hierarchies for massive neutrinos (see Eq. (54) from Ma & Bertschinger 1995) at $l_{max} = 15$ for every q value. We then gradually increase these numbers until $N_{q_{max}} = 100$ and $l_{max} = 50$ for testing the numerical precision and obtaining a relative accuracy better than 10^{-3} for the models with oscillations and without oscillations.

Fig. 1 presents the dependence of the CMB anisotropy and polarization power spectra on the neutrino difference of the squared masses Δm^2, the vacuum mixing angle $\sin^2 2\theta_0$ and the lepton asymmetry L_ν, obtained in a ΛCHDM model having: $\Omega_b = 0.023$, $\Omega_\Lambda = 0.7$, $\Omega_c = 1 - \Omega_b - \Omega_\nu - \Omega_\Lambda$, $h_0 = 0.65$. For all cases we assume a total neutrino mass $m_\nu = m_{\nu_\mu} + m_{\nu_\tau} = 0.6$eV and a total neutrino degeneracy parameter $\xi_\nu = \xi_{\nu_\mu} + \xi_{\nu_\tau} = 5$. We also assume a primordial scale-invariant power spectrum, the presence of the scalar modes with spectral index $n_s = 1$ and a standard ionization history of the universe. All the power spectra are normalized to COBE/DMR four-Year data (Bunn & White 1997). Panels a1) and a2) present the CMB anisotropy and polarization power spectra for $\sin^2 2\theta_0 = 0.8$, $\Delta\xi_\nu = \xi_{\nu_\tau} - \xi_{\nu_\mu} = 4$ ($L_\nu = 3.54$) and some values of Δm^2. Panels b1) and b2) show the same power spectra for $\Delta m^2 = 0.24$eV^2, $\Delta\xi_\nu = 4$, and some values of $\sin^2 2\theta_0$. Panels c1) and c2) present the CMB anisotropy and polarization power spectra for $\Delta m^2 = 0.24$eV^2, $\sin^2 2\theta_0 = 0.45$ and $\Delta\xi_\nu/L_\nu =$ 0/2.03, 1/2.13, 3/2.88, 4/3.54. For all cases

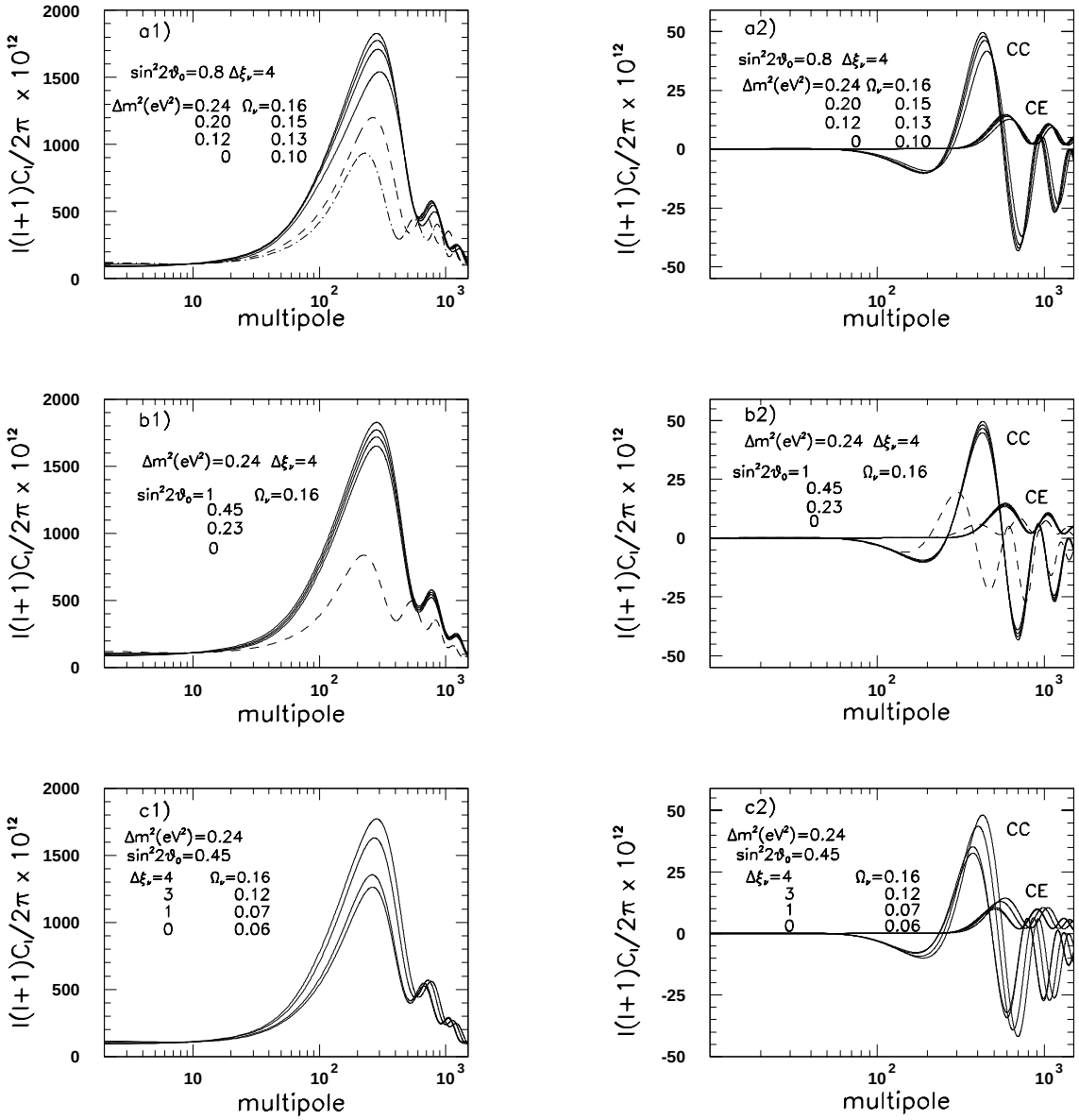

Fig. 1. The dependence of CMB anisotropy (left panels) and polarization (right panels) power spectra on Δm^2 (panels **a1** and **a2**) $\sin^2 2\theta_0$ (panels **b1** and **b2**) and $\Delta\xi_\nu$ (panels **c1** and **c2**) for a ΛCHDM model having: $\Omega_b = 0.023$, $\Omega_\Lambda = 0.7$, $\Omega_c = 1 - \Omega_b - \Omega_\nu - \Omega_\Lambda$, $h_0 = 0.65$, $m_\nu = m_{\nu_\mu} + m_{\nu_\tau} = 0.6$eV, $\xi_\nu = \xi_{\nu_\mu} + \xi_{\nu_\tau} = 5$. As a consistency test we present in panel a1) the CMB anisotropy power spectra obtained for degenerate neutrinos with: $m_\nu = 0.07$eV, $\xi_\nu = 3$ (dashed line), $m_\nu = 0.07$eV, $\xi_\nu = 0$ (dash-dotted line) and $h_0 = 0.65$, $\Omega_b = 0.05$, $\Omega_\Lambda = 0.7$, $\Omega_c = 1 - \Omega_b - \Omega_\nu - \Omega_\Lambda$. In panels **b1** and **b2** we present (dashed lines) the CMB angular power spectra obtained for: $\Omega_\nu \approx 0.015$, $\xi_\nu = 0$, $\Omega_b = 0.023$, $\Omega_\Lambda = 0.7$, $\Omega_c = 0.262$, $h_0 = 0.65$, one massless and two massive neutrino species (see also the text). We choose such values of neutrino oscillation parameters in order to clearly see the neutrino oscillation effects on CMB power spectrum.

we indicate the corresponding values of Ω_ν (Eq. 17). Without oscillations our power spectra are in agreement with the CMB anisotropy power spectra presented by Lesgourgues & Pastor 1999. Also, in panels b1) and b2) we present (dashed lines) the CMB angular power spectra obtained for: $\Omega_\nu \approx 0.015$, $\xi_\nu = 0$, $\Omega_b = 0.023$, $\Omega_\Lambda = 0.7$, $\Omega_c = 0.262$, $h_0 = 0.65$, one massless and two massive neutrino species. We check that our results match exactly those obtained by using the unmodified version of the CMBFAST code.

The power spectra presented in Fig. 1 show two distinct features: a vertical shift of the C_l at large l (present in all panels) with the increasing of Δm^2, $\sin^2 2\theta_0$ and $\Delta\xi_\nu$ values, that results from the modification of neutrino free streaming scales, and an horizontal shift of the Doppler peaks to lower l when Δm^2 and $\Delta\xi_\nu$ are increased, that results from the increase of the sound horizon at recombination. The horizontal shift of C_l is not present in panels b1) and b2) because the variation of $\sin^2 2\theta_0$, with Δm^2 and $\Delta\xi_\nu$ kept fixed, does not change Ω_ν

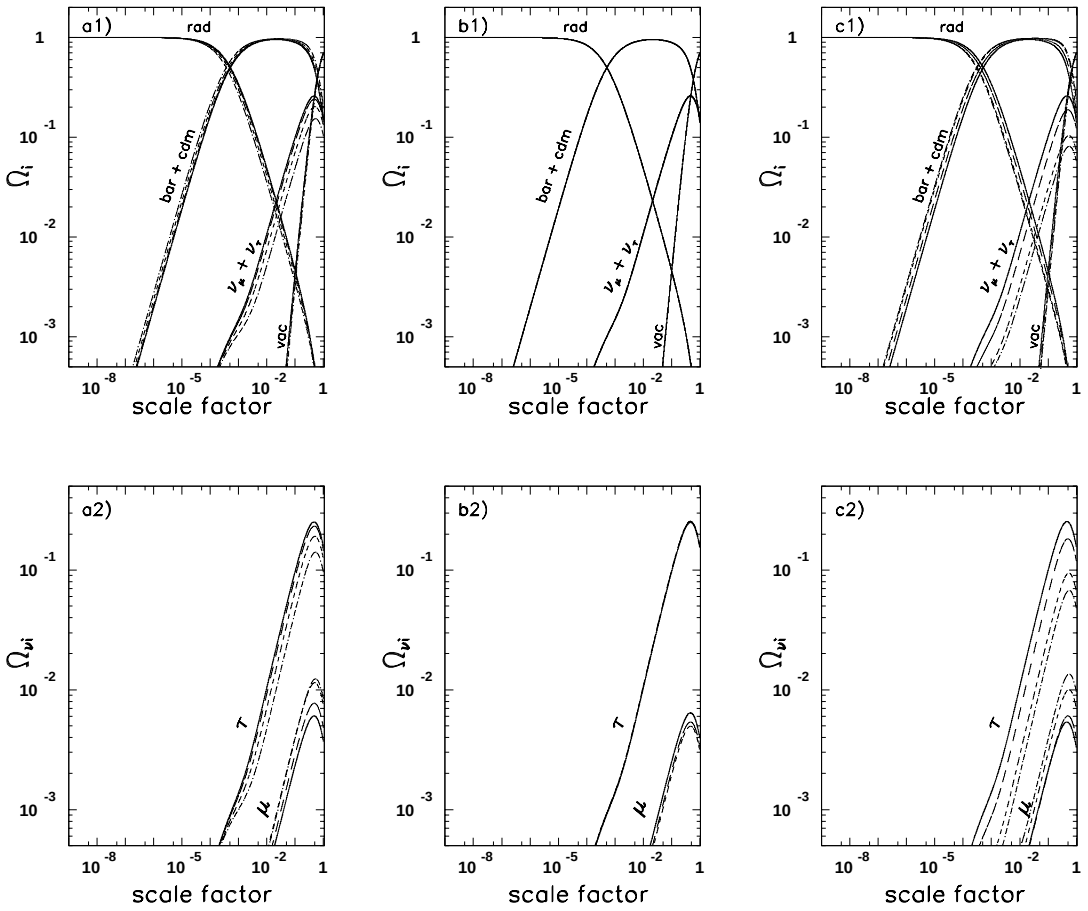

Fig. 2. The evolution with the scale factor of the energy densities, relative to the critical density, of the various components, for the models presented in Fig. 1. Panel **a**: $\sin^2 2\theta_0 = 0.8$, $\Delta\xi_\nu = 4$ ($L_\nu = 3.54$) and Δm^2: 0.24eV^2 (continuous lines), 0.2eV^2 (long-dashed lines), 0.12eV^2 (dashed lines), 0 (dott-dashed lines). Panel **b**: $\Delta m^2 = 0.24$eV^2, $\Delta\xi_\nu = 4$ ($L_\nu = 3.54$) and $\sin^2 2\theta_0$: 0, 0.23, 0.45, 1 (see also the text). Panel **c**: $\Delta m^2 = 0.24$, $\sin^2 2\theta_0 = 0.45$ and $\Delta\xi_\nu/L_\nu$: 4/3.54 (continuous lines), 3/2.88 (long-dashed lines), 1/2.13 (dashed lines), 0/2.03 (dott-dashed lines). Panels **a1**, **b1** and **c1** show the separate contributions from the two types of massive neutrinos (together with antineutrinos) for the same cases of the above panels. For all values of the scale factor, $\sum_i \Omega_i = 1$.

and consequently the Hubble expansion rate is not changed. (see Eqs. 14 and 15).

For a better understanding of these features, Fig. 2 shows the evolution with the scale factor of the energy densities, relative to the critical density, of the various components (Ω_{cdm} for CDM, Ω_{bar} for baryons, Ω_{rad} for radiation in the form of one massless neutrino and photons, Ω_{ν_μ} and Ω_{ν_τ} for the massive neutrinos and antineutrinos, Ω_{vac} for vacuum), for the models presented in Fig. 1. Panel a) presents the evolution with the scale factor of Ω_i for $\sin^2 2\theta_0 = 0.8$, $\Delta\xi_\nu = 4$ ($L_\nu = 3.54$) and some values of Δm^2. The same time evolution is presented in panel b) for $\Delta m^2 = 0.24\text{eV}^2$, $\Delta\xi_\nu = 4$ ($L_\nu = 3.54$) and some values of $\sin^2 2\theta_0$. In these cases, as consequence of the conservation of the Hubble expansion rate for all values of the scale factor, the time evolution of Ω_i do not changes with the variation of $\sin^2 2\theta_0$. Panel c) presents the evolution with the scale factor of Ω_i for $\Delta m^2 = 0.24$, $\sin^2 2\theta_0 = 0.45$ and some values of $\Delta\xi_\nu/L_\nu$. Panels a1), b1) and c1) show the separate contributions from the two types of massive neutrinos for the same cases of the above panels. For all values of the scale factor, $\sum_i \Omega_i = 1$.

Fig. 3 shows the time evolution (in synchronous gauge) of the perturbed energy density of the density field components. The left panels of Fig. 3 present the evolution with the scale factor of the perturbed energy density of different density field components in the presence of neutrino oscillations (δ_{cdm} for CDM, δ_{bar} for baryons, δ_{rad} for radiation in the form of massless neutrino and photons, δ_{ν_μ} for ν_μ plus $\bar\nu_\mu$ and δ_{ν_τ} for ν_τ plus $\bar\nu_\tau$), for the mode $k \approx 0.2\text{Mpc}^{-1}$. The right panels of Fig. 3 present, for the same mode k, the evolution with the scale factor of the quantity $\epsilon = \sigma_{\nu_1} - \sigma_{\nu_2}$ (proportional with the variation of the massive neutrinos shear stress), where σ_{ν_1} and σ_{ν_2} are:

$$\sigma_{\nu_1} = \sum_i \frac{\delta\rho_i}{\rho_i + P_i}, \quad (i = \nu_\tau, \bar\nu_\tau \;\; j = \nu_\mu, \bar\nu_\mu)$$
$$\sigma_{\nu_2} = \sum_j \frac{\delta\rho_j}{\rho_j + P_j} \tag{18}$$

Here ρ_ν and P_ν are the neutrino/antineutrino energy density and pressure and $\delta\rho_\nu$ is the perturbation of neutrino/antineutrino

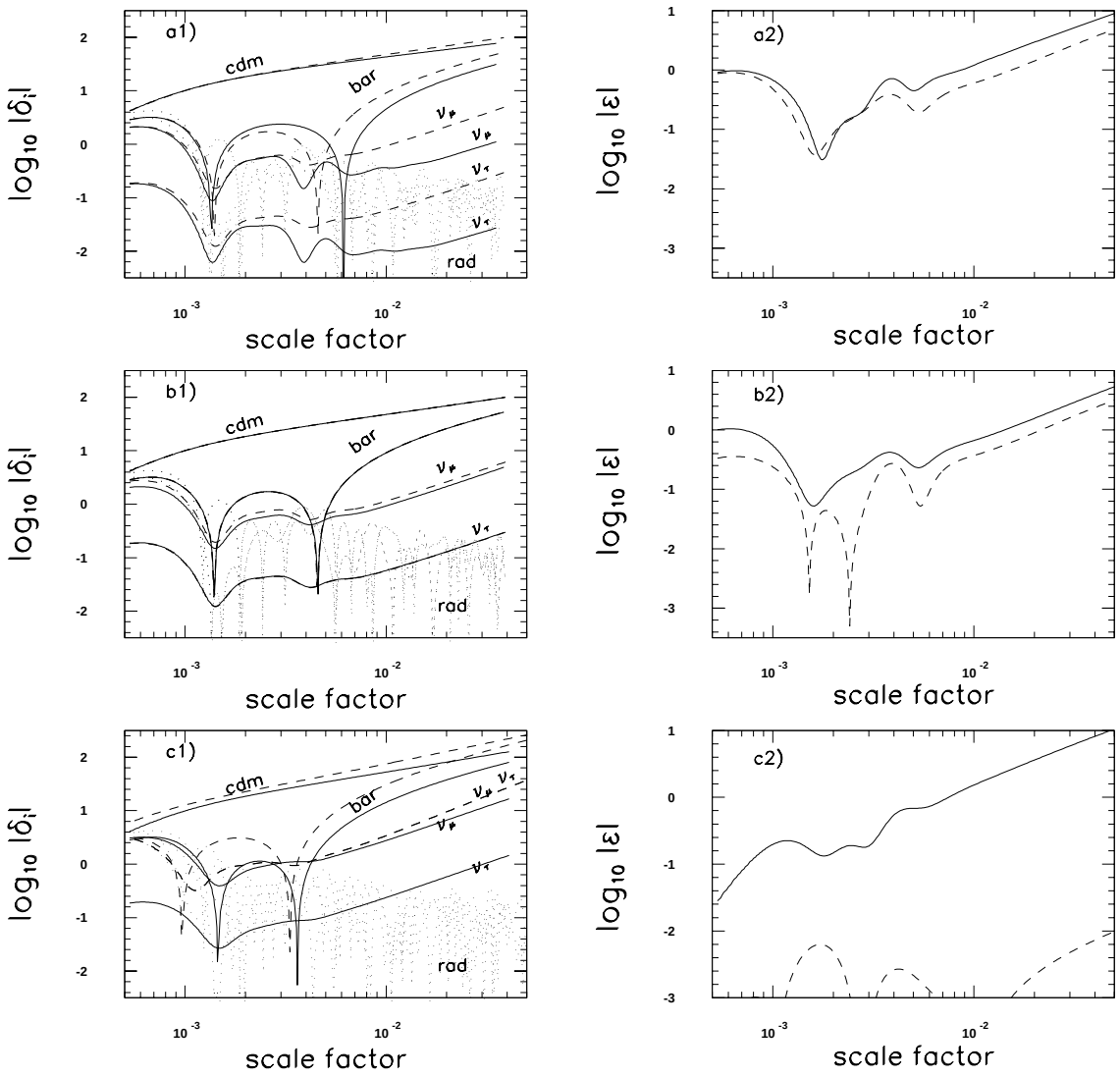

Fig. 3. The evolution with the scale factor (in synchronous gauge) of the density perturbations (left panels) and of $\epsilon = \sigma_{\nu_1} - \sigma_{\nu_2}$ (see also the text) for the mode $k \approx 0.2\mathrm{Mpc}^{-1}$. Panels **a1** and **a2**: $\sin^2 2\theta_0 = 0.8$, $\Delta\xi_\nu = 4$ and $\Delta m^2 = 0.24\mathrm{eV}^2$ (continuous line) and $\Delta m^2 = 0.12\mathrm{eV}^2$ (dashed line); Panels **b1** and **b2**: $\Delta m^2 = 0.12\mathrm{eV}^2$, $\Delta\xi_\nu = 4$ and $\sin^2 2\theta_0 = 0.8$ (continuous line) and $\sin^2 2\theta_0 = 0.23$ (dashed line); Panels **c1** and **c2**: $\Delta m^2 = 0$, $\sin^2 2\theta_0 = 0$,$\Delta\xi_\nu = 4$ (continuous line) and $\Delta m^2 = 0$, $\sin^2 2\theta_0 = 0$, $\Delta\xi_\nu = 0$ (dashed line). For all cases the total neutrino mass is $m_\nu = 0.6$eV, the total neutrino degeneracy parameter is $\xi_\nu = 5$ and the cosmological model is the ΛCHDM model presented in Fig. 1.

energy density. For all cases the total neutrino mass is $m_\nu = 0.6$eV, the total neutrino degeneracy parameter is $\xi_\nu = 5$ and the cosmological model is the ΛCHDM model presented in Fig. 1. In panels a1) and a2) of Fig. 3 $\sin^2 2\theta_0 = 0.8$ and $\Delta\xi_\nu = 4$ are fixed, and $\Delta m^2 = 0.24\mathrm{eV}^2$ (continuous line) and $\Delta m^2 = 0.12\mathrm{eV}^2$ (dashed line). In panels b1) and b2) of the same figure $\Delta m^2 = 0.12\mathrm{eV}^2$ and $\Delta\xi_\nu = 4$ are fixed and $\sin^2 2\theta_0 = 0.8$ (continuous line), $\sin^2 2\theta_0 = 0.23$ (dashed line). We observe that the growth of δ_{ν_i} is suppressed when Δm^2 and $\sin^2 2\theta_0$ values are increased, while the variation of neutrino shear stress gets larger with the increasing of these parameters. In panels c1 and c2 of Fig. 3 $\Delta m^2 = 0$, $\sin^2 2\theta_0 = 0$ and $\Delta\xi_\nu = 4$ (continuous line) and $\Delta m^2 = 0$, $\sin^2 2\theta_0 = 0$ and $\Delta\xi_\nu = 0$ (dashed line). For this last case, $\delta\rho_{\nu_\mu} \approx \delta\rho_{\nu_\tau}$ and $|\epsilon| < 10^{-2}$.

4. Detection of neutrino oscillations with CMB experiments

Different methods can be used to quantify the performance of a CMB experiment in measuring a given set of cosmological parameters. We estimate the errors on the oscillation parameters Δm^2 and $\sin^2 2\theta_0$ and the lepton asymmetry L_ν by using the Fisher information matrix approximation, widely employed in the literature (e.g. Efstathiou & Bond 1999; Popa et al. 1999).

The Fisher information matrix elements F_{ij} measure the width and the shape of the likelihood function around its maximum (Efstathiou & Bond 1999). The minimum error that can be obtained on a parameter s_i when we need to determine all parameters jointly, is given by:

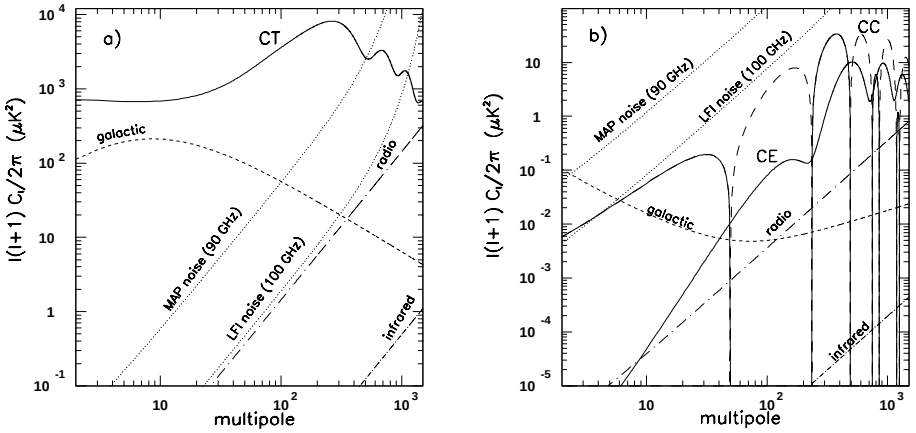

Fig. 4. Temperature (left panel) and polarization (right panel) power spectra for the neutrino oscillation target model considered here (see also the text) compared to astrophysical component power spectra: the galactic temperature fluctuations at moderate galactic latitudes, sum of synchrotron, free-free and dust fluctuations, and the extragalactic source temperature fluctuations modelled as in Toffolatti et al. (1998) and De Zotti et al. (1999a) and the polarization fluctuations from galactic synchrotron and dust emission and separately from extragalactic radiosources and infrared sources modelled according to De Zotti et al. (1999b) and references therein. We report also the white noise nominal power spectrum for LFI and MAP, taking into account the effect of resolution loss at high l due to the beam convolution.

$$\delta s_i = \sqrt{F_{ii}^{-1}}, \tag{19}$$

depending on the experimental parameter data set and the target model and the class of considered cosmological models.

If only the temperature anisotropy power spectrum C_{Tl} is used, the Fisher information matrix reads as (Efstathiou & Bond 1999):

$$F_{ij} = \sum_l \frac{\delta \hat{C}_{Tl}}{\delta s_i} \cdot Cov^{-1}(C_{Tl}^2) \cdot \frac{\delta C_{Tl}}{\delta s_j}. \tag{20}$$

If both anisotropy and polarization power spectra are used, the Fisher information matrix is given by (Zaldarriaga & Seljak 1997; Zaldarriaga 1997):

$$F_{ij} = \sum_l \sum_{X,Y} \frac{\partial C_{Xl}}{\partial s_i} Cov^{-1}(\hat{C}_{Xl}, \hat{C}_{Yl}) \frac{\partial C_{Yl}}{\partial s_j}, \tag{21}$$

where: X and Y stands for T, E, C and B power spectra and Cov^{-1} is the inverse of the covariance matrix. For the purpose of this work we assume only scalar modes, then the relevant covariance matrix elements in Eqs. (21) ÷ (23) are:

$$\begin{aligned}
Cov(\hat{C}_{Tl}^2) &= \frac{2}{(2l+1)f_{sky}}(C_{Tl} + w_T^{-1}B_{Tl}^{-2})^2, \\
Cov(\hat{C}_{El}^2) &= \frac{2}{(2l+1)f_{sky}}(C_{El} + w_P^{-1}B_{Pl}^{-2})^2, \\
Cov(\hat{C}_{Cl}^2) &= \frac{2}{(2l+1)f_{sky}} \\
&\quad \times [C_{Cl}^2 + (C_{Tl} + w_T^{-1}B_{Tl}^{-2})(C_{El} + w_P^{-1}B_{Pl}^{-2})], \\
Cov(\hat{C}_{Tl}\hat{C}_{El}) &= \frac{2}{(2l+1)f_{sky}} C_{Cl}^2, \\
Cov(\hat{C}_{Tl}\hat{C}_{Cl}) &= \frac{2}{(2l+1)f_{sky}} C_{Cl}(C_{Tl} + w_T^{-1}B_{Tl}^{-2}), \\
Cov(\hat{C}_{El}\hat{C}_{Cl}) &= \frac{2}{(2l+1)f_{sky}} C_{Cl}(C_{El} + w_P^{-1}B_{Pl}^{-2}).
\end{aligned} \tag{22}$$

Here we set $w_T = \sum_c w_c^T$ for anisotropy and $w_P = \sum_c w_c^P$ for polarization (with the sum performed over detector channels), $w_c^T = (\sigma_c^T \theta_{c,pix})^{-2}$ and $w_c^P = (\sigma_c^P \theta_{c,pix})^{-2}$, where σ_c^T and σ_c^P are the relative noise per pixel for anisotropy and polarization channels (Knox 1995); $B_{Tl}^2 = \sum_c B_{cl}^2 w_c^T / w_T$ and $B_{Pl}^2 = \sum_c B_{cl}^2 w_c^P / w_P$ account for the beam smearing, $B_{cl}^2 = e^{-l(l+1)/l_s^2}$ is the Gaussian beam profile, $l_s = \sqrt{8 \ln 2}(\theta_c)_{fwhm}^{-1}$ and f_{sky} is the fraction of the sky used in the analysis.

Assessing PLANCK performances under realistic assumptions is a very delicate task: both instrumental systematic effects (e.g. Delabrouille 1998; De Maagt et al. 1998; Maino et al. 1999; Burigana et al. 1998 and references therein) and astrophysical contamination (e.g. Toffolatti et al. 1998, 1999; De Zotti et al. 1999a,b and references therein) have to be carefully understood, reduced by optimizing the telescope (Mandolesi et al. 1998b) and the instrumental design (Bersanelli & Mandolesi 1998; Puget et al. 1998) and accurately subtracted in the data analysis. For simplicity, we consider only the MAP and PLANCK "cosmological windows", i.e. those frequencies that are minimally affected by foregrounds contaminations, and neglect the degradation in CMB power spectrum recovering introduced by foreground contaminations and instrumental effects. As shown in Fig. 4, in the cosmological channels extragalactic source fluctuations are comparable to CMB ones only at $l > 10^3$, both for temperature (left panel) and polarization (right panel) anisotropies, whereas galactic fluctuations, which power spectrum overwhelms the extragalactic foreground one at $l \lesssim 10^2$, are below the CMB ones at least far from the galactic plane.

Then, the possible imprinting of neutrino oscillations in the CMB anisotropy are not significantly masked from astrophysical contaminations at frequencies $\sim 70 \div 200$ GHz. We exploit then separately different sets of PLANCK data: the "cosmological" LFI channels alone (70 and 100 GHz channels), the

Table 1. Summary of instrumental performances of future CMB space missions in their "cosmological channels". For MAP and PLANCK LFI we compute $\sigma_c^P = \sqrt{2}\sigma_c^T$ (Zaldarriaga & Seljak 1997).

Instrument	ν(GHz)	θ_{fwhm}	$\sigma_c^T/(\mu K/K)$	$(w_c^T)^{-1}/10^{-15}$	$\sigma_c^P/(\mu K/K)$	$(w_c^P)^{-1}/10^{-15}$
MAP	60	$21'$	12.1	5.4	17.11	10.92
(Bennett et al. 1996b)	90	$12.6'$	25.5	8.7	36.06	17.46
PLANCK LFI	70	$14'$	3.6	0.215	5.09	0.429
(Mandolesi et al. 1998a)	100	$10'$	4.3	0.156	6.08	0.312
PLANCK HFI	100	$10.7'$	1.7	0.028		
(Puget et al. 1998)	143	$8'$	2.0	0.022	3.7	0.074
	217	$5.5'$	4.3	0.047	8.9	0.020

"cosmological" HFI channels alone (143 and 217 GHz channels and 100 GHz but for the temperature fluctuations only) and both together. For comparison, we consider also the set of data from the two MAP "cosmological" channels at 60 and 90 GHz. Table 1 lists the experimental parameters of the various experiments that we considered in our calculations.

The PLANCK and MAP data will be mainly used for determining the cosmological parameters; we exploit then the Fisher matrix method by evaluating together the uncertainties (1σ errors) of a simple set of cosmological parameters and of the parameters characterizing the neutrino oscillation model discussed here. As well known, the errors quoted for the considered parameters depend on the experiment sensitivity but also in part on the assumed target model and the set of considered parameters.

We assume as target model a spatially flat ΛCHDM model without oscillations having: $\Omega_b = 0.023$, $\Omega_\Lambda = 0.7$, $\Omega_c = 1 - \Omega_b - \Omega_\nu - \Omega_\Lambda$, $h_0 = 0.65$, $n_s = 1$, $m_\nu = m_{\nu_\mu} + m_{\nu_\tau} = 0.6$eV, $\xi_\nu = \xi_{\nu_\mu} + \xi_{\nu_\tau} = 5$, $\Delta\xi_\nu = 1$ ($L_\nu = 2.13$), $\Delta m^2 = 1.24 \times 10^{-2}\mathrm{eV}^2$, and $\sin^2 2\theta_0 = 0$. We also assume a scale invariant power spectrum, the presence only of the scalar modes having a spectral index $n_s = 1$, and ignore the contribution of the tensorial modes and reionisation effects. The tensorial modes have a small contribution only to the polarization signal at low order multipoles (Crittenden & Turok 1995; Seljak 1997; Kamionkowski & Kosowsky 1998) that will be difficult to detect against the polarized foregrounds. Also, the reionisation effects can help in breaking the degeneracy only in the presence of the polarization signal for a large value of the optical depth to Thomson scattering (Zaldarriaga et al. 1997).

We numerically compute the partial derivatives of the power spectra with respect to each relevant parameter s_i by approximating them with the (possibly central) finite differences between the two power spectra obtained by varying with a quantity $\pm\Delta s_i/2$ the parameter s_i in consideration around its value $s_{i,0}$ assumed in the considered target model. Typically, Δs_i is taken in the range between few percent, in order to have a step small enough for an accurate evaluation of the derivative and large enough for having quite sensitive and numerically stable variations of the power spectrum.

Table 2 presents 1-σ errors on the estimates of the relevant cosmological parameters and neutrino oscillation parameters obtained from the anisotropy alone and anisotropy plus polarization, for the experimental parameters listed in Table 1 and few values of f_{sky}. The errors presented in Table 2 arise because of the geometrical degeneracy (see Efstathiou & Bond 1999 and the references therein) that imposes limits on the determination of h_0 and Ω_Λ, and the correlations existing among the energy density parameters and n_s and $\sin^2 2\theta_0$.

Table 3. 1σ errors on the estimates of the neutrino oscillation parameters and lepton asymmetry obtained from anisotropy and polarization power spectrum statistics.

f_{sky}		1.	0.8	0.65
MAP	$\delta L_\nu/L_\nu \times 10^2$	1.21	1.35	1.50
	$\delta\Delta m^2/\Delta m^2$	4.08	4.56	5.06
	$\delta \sin^2 2\theta_0$	0.68	0.77	0.85
PLANCK	$\delta L_\nu/L_\nu \times 10^3$	2.13	2.38	2.64
	$\delta\Delta m^2/\Delta m^2$	0.79	0.88	0.97
	$\delta \sin^2 2\theta_0$	0.13	0.19	0.21

These errors can be understood in terms of the ability of each experiment to determine the properties of Doppler peaks (Efstathiou & Bond 1999): the location of the first Doppler peak and the positions, heights and relative amplitudes of the first and subsidiary Doppler peaks. The Doppler peak positions l_d [$l_d \approx m\pi d_A(z)/r_s$, where $d_A(z)$ is the angular diameter distance to the last scattering, r_s is the sound horizon distance and m is the Doppler peak number] suffer the degeneracy between Ω_Λ and h_0 when Ω_m is fixed ($\Omega_m = \Omega_b + \Omega_c + \Omega_\nu = 0.3$). From Eq. (19) Ω_ν value is given by the Δm^2 and L_ν values when the total neutrino mass is fixed, and therefore Δm^2 and L_ν are also correlated. The Doppler peak heights suffer the degeneracy between Ω_c, Ω_b, Ω_ν, n_s and $\sin^2 2\theta_0$.

Clearly, the PLANCK LFI, probing the subsidiary Doppler peaks structure to high multipoles $l \sim 1500$, will produce a significant improvement with respect to MAP (sensitive up to $l \sim 1000$) in the determination of all parameters reducing their uncertainties. A further improvement can be achieved by exploiting the better sensitivity and angular resolution (up to $l \sim 2000$) of PLANCK HFI, the full PLANCK performance at very high l being limitated essentially by the foreground contamination.

On the other hand, other kinds of astronomical observations provide information on the cosmological parameters, complementary to those derived from CMB anisotropies. Galaxy clus-

Table 2. 1σ errors on the estimates of the cosmological parameters and neutrino oscillation parameters obtained from the power spectrum statistics.

		Anisotropy			Anisotropy & polarization		
f_{sky}		1.	0.8	0.65	1.	0.8	0.65
	$\delta n_s \times 10^2$	1.44	1.61	1.79	1.30	1.46	1.62
	$\delta\Omega_\Lambda/\Omega_\Lambda \times 10^2$	6.01	6. 71	7.45	5.13	5.73	6.36
	$\delta\Omega_b/\Omega_b$	0.20	0.22	0.25	0.16	0.18	0.20
MAP	$\delta h_0/h_0$	0.11	0.13	0.14	0.10	0.12	0.13
	$\delta L_\nu/L_\nu$	0.24	0.27	0.29	0.21	0.24	0.26
	$\delta\Delta m^2/\Delta m^2$	11.91	13.31	14.77	10.03	11. 22	12.45
	$\delta \sin^2 2\theta_0$	1.42	1.59	1.76	1.42	1.59	1.76
	$\delta n_s \times 10^3$	4.69	5.24	5.81	2.46	2.76	3.06
	$\delta\Omega_\Lambda/\Omega_\Lambda \times 10^2$	2.24	2.50	2.78	0.99	1.11	1.23
	$\delta\Omega_b/\Omega_b \times 10^2$	4.99	5.58	6.19	1.95	2 .18	2.42
PLANCK-LFI	$\delta h_0/h_0 \times 10^2$	3.26	3.65	4.05	1.66	1.86	2.06
	$\delta L_\nu/L_\nu \times 10^2$	8.13	9.08	10.08	3.97	4.44	4.93
	$\delta\Delta m^2/\Delta m^2$	3.52	3.94	4.37	2.16	2.42	2.68
	$\delta \sin^2 2\theta_0$	0.64	0.72	0.79	0.63	0.70	0.78
	$\delta n_s \times 10^3$	1.84	2.06	2.28	0.95	1.06	1.18
	$\delta\Omega_\Lambda/\Omega_\Lambda \times 10^3$	9.18	10.26	11.38	4.09	4.57	5.07
	$\delta\Omega_b/\Omega_b \times 10^2$	1.80	2.01	2.23	0.64	0.72	0.80
PLANCK-HFI	$\delta h_0/h_0 \times 10^2$	1.74	1.95	2.16	0.64	0.72	0.79
	$\delta L_\nu/L_\nu \times 10^2$	4.09	4.57	5.07	1.63	1.84	2.04
	$\delta\Delta m^2/\Delta m^2$	2.11	2.35	2.61	1.39	1.56	1.73
	$\delta \sin^2 2\theta_0$	0.41	0.46	0.51	0.37	0.41	0.46

ter observations limit the shape parameter Γ and the normalization of the galaxy power spectrum σ_8 and, combined with the galaxy peculiar velocity fields, provide informations on the matter density in the universe Ω_m (Dekel 1994; Strauss & Willick 1995). Weak gravitational lensing provides also direct estimates of q_0 (see e.g Seljak 1998). The ratio between baryon and total mass in clusters $\Omega_b/\Omega_m \approx (0.01 - 0.02)\, h_0^{-2}$ (see e.g. Dodelson et al. 1996 and the references therein), informations from the BBN [$\Omega_b = 0.02 h_0^{-2}$ (Burles & Tytler 1998)] and the Helium Lyman-Alpha Forest (Wadsley et al. 1999) constrain Ω_m or h_0 if Ω_m is known from other kinds of measurements. The complementarity between Type 1a supernovae luminosity distances and CMB anisotropy provides a powerful tool in breaking the degeneracy between Ω_k and Ω_Λ (see e.g. Perlmutter et al. 1997; Efstathiou & Bond 1999; Efstathiou et al. 1999 and the references therein). The ages of the oldest globular clusters set lower limits on the age of the universe (see e.g. Chaboyer 1998) and then on Ω_k and Ω_Λ if Ω_m is well constrained. For a spatially flat universe this contributes to break the geometrical degeneracy in h_0 - Ω_Λ plane. For CDM models with known baryonic content, measurements of Γ from large scale structure, combined with independent determinations of Ω_m, provide estimates on h_0 (Efstathiou & Bond 1999). Constraints on the scalar spectral index n_s can be inferred also from limits on the primordial black hole abundance (Green et al. 1997) and on the CMB spectral distortions (Hu et al. 1994).

Recent CMB anisotropy measurements from BOOMERANG and MAXIMA-1 have been in fact used jointly to other astronomical observations to determine cosmological parameters through the so-called analysis with prior (Lange et al. 2000; Balbi et al. 2000). Of course, adding information from other kind of observations helps both in circumventing the degeneracy problem and in improving the accuracy in the determination of the cosmological parameters.

Such a kind of analysis is out of the aim of this work. We just estimate here lower limits on the MAP and PLANCK sensitivity in determining the neutrino oscillation parameters, by exploiting the Fisher matrix method, assuming that all the cosmological parameters are known and estimating only the joint errors on Δm^2, $\sin^2 2\theta_0$, and L_ν that can be obtained from CMB anisotropy plus polarization data.

Table 3 presents these errors (1σ errors) for PLANCK (LFI and HFI together) and MAP experiments; together with the results shown in Table 2, it provides a range of PLANCK and MAP sensitivity to neutrino oscillation parameters. Of course, in this case we find a significant reduction of the errors on the neutrino oscillation parameters for both PLANCK and MAP. These values can be also considered as estimates of lower limits on the errors on the neutrino oscillation parameters, as they could be in principle stetted by PLANCK and MAP experiments.

Fig. 5 presents few confidence regions of the neutrino oscillation parameters space that can be potentially detected by the PLANCK surveyor and few allowed regions of Δm^2 and $\sin^2 2\theta_0$ at the same confidence level (CL) obtained by MACRO Collaboration (Ambrosio et al. 1998).

According to the standard χ^2 method (see e.g Particle Data Group 1998) an input model defined by the parameters (Δm^2, $\sin^2 2\theta_0$) is more likely to have occurred higher is the proba-

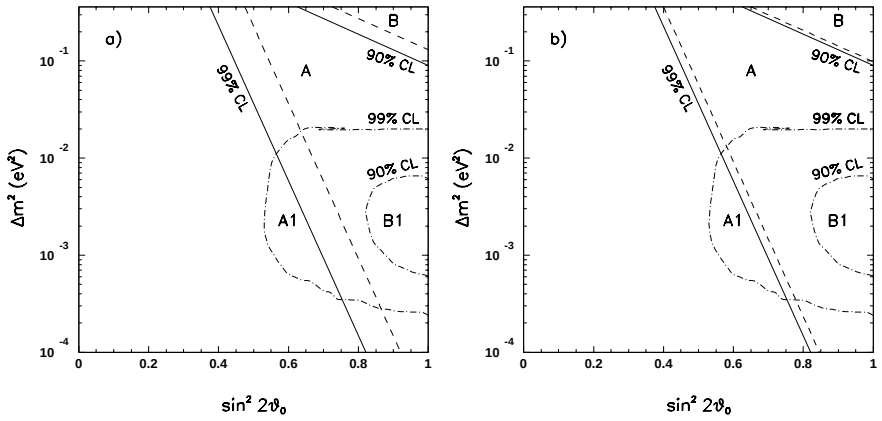

Fig. 5a and b. Confidence regions of the neutrino oscillation parameter space that can be potentially detected by PLANCK surveyor by using CMB anisotropy measurements. Panel **a**: the allowed confidence regions at 99% CL (A) and at 90% CL (B) obtained for $f_{sky} = 0.65$ (continuous lines) and $f_{sky} = 0.8$ (dashed lines). The target model has $\Delta m^2 = 1.24 \times 10^{-2}\mathrm{eV}^2$ and $\sin^2 2\theta_0 = 0$ (see also the text). Panel **b**: the allowed confidence regions at 99% CL (A) and at 90% CL (B) for $f_{sky} = 0.65$. The target model has: $\Delta m^2 = 1.24 \times 10^{-2}\mathrm{eV}^2$ and $\sin^2 2\theta_0 = 0$ (continuous lines) and $\Delta m^2 \approx 10^{-4}\mathrm{eV}^2$ and $\sin^2 2\theta_0 = 0$ (dashed lines). In each panel we also present (dash-dotted lines) the allowed regions of Δm^2 and $\sin^2 2\theta_0$ at 99% CL (A1) and 90% CL (B1) measured by the MACRO experiment.

bility to obtain χ^2 values larger than a specific value χ_0^2. The cumulative probability that defines a certain confidence region on the parameters is given by:

$$CL(\chi_0^2) = \int_{\chi_0^2}^{\chi^2_{max}} L(\chi^2, \Delta m^2, \sin^2 2\theta_0) d\chi^2, \qquad (23)$$

where $\chi_0^2 = \chi^2_{min} + \Delta\chi^2$, with $\Delta\chi^2 = 4.61, 9.21$ at 90% and 99% CL respectively (for a χ^2 distribution with two degrees of freedom). The likelihood function in the Eq. (25) is defined as (Efstathiou & Bond 1999):

$$-2\ln\left(\frac{L}{L_{max}}\right) = \sum_{l<l_{max}} \frac{(C_l(s) - C_l(s0))^2}{Cov(\hat{C}^2_{Tl})},$$

where $C_l(s_0)$ is the power spectrum for the target model, $C_l(s)$ is the power spectrum for the input model having the same cosmological parameters as the target model and Δm^2 and $\sin^2 2\theta_0$ are in the intervals $(0 - 0.36)\mathrm{eV}^2$ and $(0 - 1)$ respectively.

Panel a) of Fig. 5 presents the confidence regions that could be obtained with the PLANCK surveyor for different fractions of sky. The target model is the $\Lambda CHDM$ model used in the previous section. Panel b) of the same figure presents the confidence regions obtained with PLANCK for $f_{sky} = 0.65$ and the same target model and for another target model.

In each panel we also present the allowed regions of Δm^2 and $\sin^2 2\theta_0$ as derived from the MACRO experiment.

We conclude that exists a significant overlap between the region of the oscillation parameter space that can be potentially detected by PLANCK surveyor and that implied by the atmospheric neutrino oscillations data.

5. Conclusions

The imprint of relic degenerated neutrino oscillations on the Cosmic Microwave Background (CMB) angular power spectra is evaluated in a ΛCHDM model consistent with the structure formation theories, allowing in the same time a pattern of neutrino masses consistent with the atmospheric neutrino oscillations data.

Under the assumption that the total neutrino mass is known, as derived by the galaxy redshift surveys (Hu et al. 1998), we show that oscillations occurring between two active degenerated neutrino flavors leave detectable imprints on the CMB anisotropy and polarization power spectra.

By using the CMB anisotropy measurements, we find that the relic degenerated neutrino oscillations can be detected by PLANCK surveyor at 1σ level if the present value of the lepton asymmetry is $L_\nu \geq 9.7 \times 10^{-2}$, the difference of the neutrino squared masses is $\Delta m^2 \geq 2.91 \times 10^{-2}\mathrm{eV}^2$ and the vacuum mixing angle is $\sin^2 2\theta_0 \geq 0.46$, when we consider other cosmological parameters that simultaneously affect the CMB angular power spectra and a sky coverage of $f_{sky} = 0.8$. A slight improvement can be obtained by using the CMB anisotropy and polarization data.

Assuming that all the other cosmological parameters may be known from other kind of astronomical observations, we estimate lower limits on future CMB anisotropy and polarization experiment sensitivity in determining the neutrino oscillation parameters alone: as shown in Table 3, the errors on neutrino oscillation parameters decrease at least by a factor two with respect to the case in which no prior on cosmological parameters are assumed. These values provide estimates of lower limits on the errors on the neutrino oscillation parameters, as they could be in principle stetted by PLANCK and MAP experiments.

Finally, we compare the confidence regions of the neutrino oscillation parameter space that can be potentially detected by the PLANCK surveyor with the few allowed regions of Δm^2 and $\sin^2 2\theta_0$ obtained by MACRO Collaboration (Ambrosio et al. 1998). We find a significant overlap between the region of the oscillation parameter space that can be potentially detected by PLANCK.

Acknowledgements. We acknowledge the use of the CMBFAST Boltzmann code (version 2.4.1) developed by U. Seljak and M. Zaldarriaga. We gratefully thank the long-standing, very fruitful collaboration on PLANCK performances and on foregrounds with M. Bersanelli, L. Danese, G. De Zotti, D. Maino and L. Toffolatti. It is a pleasure to thank K. Enqvist, G. Giacomelli, R. Lopez, M. Maris and G. Venturi for useful and constructive discussions on neutrino oscillations. We wish to thank the referee for constructive comments. Part of this work was supported by NATO-CNR Fellowship Programme.

References

Ambrosio M., Atolini R., Arano C., et al. (MACRO Collab.), 1998, Phys. Lett. B 434, 451
Athanassopoulos C., Auerbach L.B., Burman R.L., et al., 1998, Phys. Rev. Lett. 81, 1744
Bahcall J.N., Krastev P.I., Smirnov, A.Yu., 1998, Phys. Rev. D58, 096016
Balbi A., Ade P., Bock J., et al., 2000, preprint astro-ph/0005124
Bennett C.L, Banday A.J., Górski K.M., et al., 1996a, ApJ 464, L1
Bennett C., et al., 1996b, Amer. Astro. Soc. Meet., 88.05
Bersanelli M., Mandolesi N., 1998, Astron. Lett. Comm., in press
Bunn E.F., White M., 1997, ApJ 480, 6
Burigana C., Maino D., Mandolesi N., et al., 1998, A&AS 130, 551
Burles S., Tytler D., 1998, Space Sci. Rev. 84, 65
Chaboyer B., 1998, preprint astro-ph/9808200
Crittenden J.R., Turok N., 1995, Phys. Rev. Lett. 75, 2642
Dekel A., 1994, ARA&A 32, 319
Delabrouille J., 1998, A&AS 127, 555
De Maagt P., Polegre A.M., Crone G., 1998, PLANCK – Straylight Evaluation of the Carrier Configuration, Technical Report ESA, PT-TN-05967, 1/0
De Zotti G., Toffolatti L., Argüeso Gómez F., et al., 1999a, In: Maiani L., Melchiorri F., Vittorio N. (eds.) Proc. 3K Cosmology: EC-TMR Conference 1999, AIP Conf. Proc., p. 204, astro-ph/9902103
De Zotti G., Gruppionio C., Ciliegi P., et al., 1999b, New Astronomy 4, 481
Dodelson S., Gyuk G., Turner M., 1994, Phys. Rev. D 49, 5068
Dodelson S., Gates I.G., Turner M., 1996, Sci 274, 69
Enqvist K., Kainulainen K., Thomson M., 1992, Nucl. Phys. B 373, 8
Efstathiou G., Bridle S.L., Lasenby A.N., et al., 1999, MNRAS 303, L47-52
Efstathiou G., Bond J.R., 1999, MNRAS 304, 75
Foot R., Thomson M.J., Volkas R.R., 1996, Phys. Rev. D 53, 5349
Foot R., Volkas R.R., 1997, Phys. Rev. D 56, 6653
Freese K., Kolb E.W., Turner M., 1983, Phys. Rev. D 27, 1689
Fukuda Y., Hayakawa T., Ichihara E., et al. (Super-Kamiokande Collab.), 1998, Phys. Rev. Lett. 81, 1562
Fukugita M., Liu G.C., Sugiyama N., 1999, Phys. Rev. Lett. 84, 1082
Gawiser E., Silk J., 1998, Sci 280, 1405
Gawiser E., 2000, preprint astro-ph/0005475
Górski K.M., Hunshaw G., Banday A.J., et al., 1994, ApJ 430, L89
Green A.M., Liddle A.R., Riotto A., 1997, Phys. Rev. D56, 7559
Hancock S., Rocha G., Lasenby A.N., et al. 1998, MNRAS 294, L1
Hannestad S., 2000, preprint astro-ph/0005018
Hu W., Scott D., Silk J., 1994, ApJ 430, 5
Hu W., Eisenstein D.J., Tegmark M., 1998, Phys. Rev. Lett. 80, 5255
Kamionkowski M., Kosowsky A., 1998, Phys. Rev. D57, 685
Kang H., Steigman G., 1992, Nucl. Phys. B 372, 494
Kinney W.H., Riotto A., 1999, Phys. Rev. Lett. 83, 3366
Knox L., 1995, Phys. Rev. D52, 4307
Lange A.E., Ade P.A.R., Bock J.J., et al., 2000, preprint astro-ph/0005004
Larsen, G.B., Madsen J., 1995, Phys. Rev. D 52, 4282
Lesgourgues J., Pastor S., 1999, Phys. Rev. D 60, 103521
Lesgourgues J., Pastor S., Prunet S., 1999, preprint hep-ph/9912363
Ma C., Bertschinger E., 1995, ApJ 518, 2
Maino D., Burigana C., Maltoni M., et al., 1999, A&AS 140, 1
Mandolesi N., et al., 1998a, PLANCK LFI, A Proposal Submitted to the ESA
Mandolesi N., Bersanelli M., Burigana C., et al., 1998b, Astron. Lett. Comm., in press, astro-ph/9904135
Mather J.C., Fixsen D.J., Shafer R.A., Mosier C., Wilkinson D.T., 1999, ApJ 512, 511
Pal P.B., Kar K., 1999, Phys. Lett. B 451, 136
Particle Data Group, 1998, The Europ. Phys. J. C 3, 1
Perlmutter S., Aldlering G., Deustua S., et al., 1997, Nat 391, 51
Popa L.A., Stefanescu P., Fabbri R., 1999, New Astronomy 4, 59
Primack J.R., Holtzman J., Klypin A., et al., 1995, Phys. Rev. Lett. 74, 2160
Primack J.R., 1998, Sci 280, 1398
Primack J.R., Gross M., 1998, to appear in: Proceedings of the Xth Rencontres de Blois, The Birth of Galaxies. 28 June–4 July 1998, astro-ph/9810204
Puget J.L., et al. 1998, HFI for the PLANCK Mission, A Proposal Submitted to the ESA
Raffelt G.G., 1996, In: Stars as Laboratories for Fundamental Physics. The University of Chicago Press, Chicago, London
Riess A.G., Filippenko A.V., Cgallis P., et al., 1998, Astron. J. 116, 1009
Scott D., White M., 1994, In: Krauss L., Kerman P. (eds.) Proceedings of the CWRU CMB Workshop: 2 Years after COBE
Seljak U., 1997a, ApJ 482, 6
Seljak U., 1998, ApJ 506, 64
Seljak U., Zaldarriaga M., 1996, ApJ 469, 437
Smoot G., Bennett C.L., Kogut A., et al., 1992, ApJ 396, L1
Steigman G., Schramm N.D., Gunn E.J., 1977, Phys. Lett. B66, 202
Strauss M., Willick, J., 1995, Phys. Repts. 261, 271
Tegmark M., Efstathiou, G., 1996, MNRAS 281, 1297
Tegmark M., 1999, fttp://www.sns.ias.edu/max/experiments. html
Toffolatti L., Argüeso Gómez F., De Zotti G., et al., 1998, MNRAS 297, 117
Toffolatti L., De Zotti G., Argüeso Gómez F., et al., 1999, In: de Oliveira-Costa A., Tegmark M. (eds.) Proc. Intern. Conf.: Microwave Foregrounds. 1999, ASP Conf. Ser. Vol. 181, p. 153, astro-ph/9902343
Wadsley J.W., Hogan C., Anderson S., et al., 1999, preprint astro-ph/9911394
White M., Gelmini G., Silk J., 1995, Phys. Rev. D 51, 2669
Wright E.L., Smoot G.F., Kogut A., et al., 1994, ApJ 420, 1
Zaldarriaga M., Seljak U., 1997, Phys. Rev. D 55, 1830
Zaldarriaga M., 1997, Phys. Rev. D 44, 1822
Zaldarriaga M., Spergel D.N., Seljak U., 1997, ApJ 488, 1